

LIMITING SPURIOUS EVAPORATION IN CLOUDS: MAGNUSSEN AND HJERTAGER (1976)'S EDC MODEL, REVISITED

Christopher A. Jeffery *

Space and Remote Sensing Sciences (ISR-2), LANL, Los Alamos, NM

Jon M. Reisner

Atmospheric, Climate and Environmental Dynamics (EES-2), LANL, Los Alamos, NM

David Moulton

Mathematical Modeling and Analysis (T-7), LANL, Los Alamos, NM

1. INTRODUCTION

It is assumed that an intermittent eddy structure is present in the flow. Liquid and vapour is assumed to be present in a near equilibrium state in certain eddies, while gas and superheated vapour is present in other eddies. Thus the rate of evaporation is limited by the rate of heat and mass transfer between these eddies. [Magnussen and Hjertager (1979, pp. 416)]

The evaporation rate of cloud droplets mixing with entrained air at high turbulent Reynolds numbers is unresolved at the grid-scale of most models, but its accurate prediction is of consequence to the much larger scale issues of cloud radiative forcing (Stephens 2005) and indirect aerosol effects (Lohmann and Feichter 2005). The numerical prediction of subgrid evaporation is typical of a broad class of problems that involve the representation of sub-centimeter-scale microphysical interactions and aerosol transformations at resolution scales of 10 m to 100 km. Rigorous mathematical analysis based on scale-separation can provide new insights (Majda and Souganidis 2000) but its general applicability to dynamic multiscale geophysical phenomena has yet to be determined.

One approach to improve the representation of cloud processes in numerical models involves the diagnosis or prognosis of subgrid moist convection and cloud amount from resolved quantities. A variety of this class of cloud scheme utilizes assumed distributions of subgrid quantities—specified by low-order moments—to provide a self-consistent diagnosis of a variety of in-cloud average and cell-average quantities (Sommeria and Deardorff 1977; Mellor 1977; Jeffery and Austin

2003). This approach falls under the general moniker of Probability Density Function (PDF) methods.

To date, all implementations of PDF methods in sub-grid cloud modeling have employed an “instantaneous” condensation and evaporation (C&E) rate assumption to diagnose liquid water mixing ratio (q_l):

$$q_l \sim \Gamma(q_t - q_s)\{q_t - q_s\} \quad (1)$$

where $\Gamma(y) = \{0, 1\}$ for $\{y < 0, y \geq 0\}$ is a step-function, and total water mixing ratio (q_t) and saturation mixing ratio (q_s) assume a distribution of values in each grid cell. Hereafter, we refer to Eq. (1) as the Instantaneous C&E (InC&E) assumption.

This extended manuscript summarizes the results of Jeffery and Reisner (2006) pertaining to the numerical prediction of evaporation rate. It begins with the observation that the evaporation rate predicted by (i) PDF schemes that utilize the InC&E assumption, and (ii) schemes that resolve supersaturation, S , and ignore subgrid correlations, disagree. We are faced with a C&E time-scale dilemma: a choice between two common subgrid cloud modeling strategies that are, in some sense, archetypal, inherently inconsistent, and thus, unsatisfactory. The central thesis of this work is that a solution to this dilemma was discovered by Magnussen and Hjertager (1976) and has been independently developed in the combustion literature. Following Magnussen and Hjertager, we refer to the modeling approach that unifies the treatment of cloud evaporation in PDF-based and resolved- S microphysical schemes as the Eddy Dissipation Concept (EDC).

This manuscript is concerned with the isobaric evaporation rate of cloudy air and its numerical prediction as specified by the evolution of relative humidity (RH). We therefore define *evaporation rate* as the rate of evolution of the mean relative humidity, \overline{RH} , of a grid-cell with internal mixing. The definition of the C&E time-scale, τ_{efold} , follows as the e -folding time of \overline{RH} evolution.

This manuscript is organized as follows. In Sec. 2 we consider the isobar mixing of clear and cloudy air

*Corresponding author address: Christopher A. Jeffery, Los Alamos National Laboratory (ISR-2), PO Box 1663, Mail Stop D-436, Los Alamos, NM 87545, USA. Tel.: (505) 665-9169; fax: (505) 664-0362. Email: cjeffery@lanl.gov

in a single grid cell and we derive the evaporation rate predicted by (i) PDF schemes that utilize the InC&E assumption [Sec. 2a] and (ii) microphysics models that resolve S and ignore subgrid correlations [Sec. 2b]. In Sec. 2c we introduce the Damköhler number—the ratio of mixing and reaction (evaporation) time-scales—which facilitates a comparison of PDF and resolved evaporation rates for a range of atmospheric conditions. In Sec. 3 we study the evaporation rate predicted numerically by a simple 1D eddy-diffusivity model for various initial conditions and diagnosed mixing time-scales; the results of this study are shown to be consistent with Magnussen and Hjertager’s EDC model. In Sec. 4 we test the efficacy of the EDC model in the Stevens et al. (1996) scenario of cloud-front propagation and evaporation; Sec. 5 contains a summary.

2. THE C&E TIME-SCALE DILEMMA

In this section we consider the isobar mixing of clear and cloudy air in a single grid cell. The PDF scheme is assumed to describe the grid cell evolution in terms of subgrid fields $\theta_l(\mathbf{x}, t)$ and $q_t(\mathbf{x}, t)$, while the resolved scheme that is often employed in LES/CRM models uses $\theta(\mathbf{x}, t)$ (or equivalently temperature) and $q_v(\mathbf{x}, t)$. It is often assumed that the LES/CRM subgrid modeling assumption is grid-cell homogeneity, i.e. $\theta = q_v = \text{constant}$ (Krueger 1993). However, this assumption is overly restrictive; our approach here is to *formally add* subgrid turbulent mixing and evolution to a single LES/CRM grid cell which retains the symmetry between the PDF and LES/CRM approaches.

2a. The InC&E assumption and its implications

Consider, first, the C&E time-scale implied by subgrid PDF schemes that use the InC&E assumption with prognostic equations for the subgrid variance of q_t and liquid water potential temperature, θ_l , in a closed cell. Assume, furthermore, that these prognostic equations predict the evolution of variance without error, i.e. the prediction of the PDF scheme is consistent with the exact evolution of the subgrid fields $\{\theta_l(\mathbf{x}, t), q_t(\mathbf{x}, t)\}$. Then beginning with advection-diffusion equations for $\{\theta, q_v\}$, assuming molecular diffusion of q_l , linearizing fluctuations of q_s^{-1} and $q_s(T)$ about the mean and introducing a molecular diffusivity, $\kappa \geq 0$ (assumed equal for q_v and θ) leads to an equation for the variance of RH_t , $\text{var}(\text{RH}_t)$:

$$\begin{aligned} \frac{\partial \text{var}(\text{RH}_t)}{\partial t} &= -2\chi \\ \chi &\equiv \kappa |\nabla \text{RH}_t|^2, \end{aligned} \quad (2)$$

where $\text{RH}_t = q_t/q_s$, overbar denotes a spatial average and χ is the scalar dissipation rate* Equation (2) illustrates the key dynamical features of subgrid PDF schemes that utilize the InC&E assumption, namely, $\text{var}(\text{RH}_t)$ decays to zero with a turbulent mixing time-scale

$$\tau_{\text{eddy}} \equiv \text{var}(\text{RH}_t)/\chi,$$

that is unresolved and must be modeled. Thus the evaporation rate is largely determined by τ_{eddy} and is independent of the microscopic phase-change (reaction) time-scale, τ_{react} , which is assumed zero in the InC&E limit.

We are thus led to the following conclusion:

The evaporation rate of unmixed clear and cloudy air predicted by a PDF scheme and the InC&E assumption in a grid cell with internal unresolved divergenceless advective-diffusive mixing depends on τ_{eddy} and is independent of τ_{react} .

2b. Resolved evaporation rates and the C&E dilemma

High resolution cloud models, e.g. Large Eddy Simulation (LES) of clouds, and somewhat coarser resolution Cloud Resolving Models (CRMs), often explicitly resolve τ_{react} . While it is typically assumed that LES/CRM assume subgrid homogeneity, we relax this assumption here and consider an isobaric model grid cell, mixed by internal velocity \mathbf{u} and molecular diffusivity κ , that has an externally specified intra-cell flux, Φ_{flux} , and is otherwise closed, i.e. $\nabla \text{RH} = \mathbf{u} = 0$ on cell faces.

$$\begin{aligned} \frac{\partial \text{RH}}{\partial t} + \mathbf{u} \cdot \nabla \text{RH} &= -\nabla \cdot \Phi_{\text{flux}} + \kappa \nabla^2 \text{RH} + \frac{1 - \text{RH}}{\tau_{\text{react}}} \\ \tau_{\text{react}}(\mathbf{x}, t) &\equiv \frac{1}{4\pi D_v N} \frac{r + a}{r^2}, \end{aligned} \quad (3)$$

where D_v is the (assumed constant) diffusivity of water vapor, a is an accommodation length introduced for analytic convenience and the small temperature dependence of τ_{react} has been ignored.

The time-scale τ_{react} was first introduced by Squires (1952) and termed the phase relaxation time. It plays a central role in the results of Wang et al. (2003).[†] Wang et al. argue that the effective time-scale over which turbulence mixing can affect the cloud liquid water flux is $(1/\tau_{\text{react}} + 1/\tau_{\text{R}})^{-1}$ (Wang et al. 2003, pp. 270) where τ_{R} is the cloud-scale large-eddy turnover time and should not be confused with the subgrid mixing time τ_{eddy} .

*For analytic convenience we define χ as the dissipation rate of half variance. Note that Eqs. (2) and (3) both assume temperature fluctuations $T' \ll R_v \overline{T}^2 / L_v$.

[†]Note that ρ_l is non-dimensional (water density divided by air density) in Eq. (18) of Wang et al. (2003)

The behavior described by Wang et al. is consistent with all current models that resolve RH and ignore sub-grid correlations as the following proof demonstrates. We first note that these cloud parameterizations replace the subgrid spatio-temporal field $\tau_{\text{react}}(\mathbf{x}, t)$ with its grid cell average $\overline{\tau_{\text{react}}}(t)$ —an assumption that is less restrictive than assuming subgrid homogeneity. Averaging Eq. (3) with this assumption and solving the resulting ODE gives the longtime behavior

$$\overline{\text{RH}}(t) = \int^t d\xi \exp \left[- \int_{\xi}^t d\xi' \overline{\tau_{\text{react}}}^{-1}(\xi') \right] \left\{ \frac{1}{\overline{\tau_{\text{react}}}(\xi)} - \frac{1}{V} \int d\lambda \hat{\mathbf{x}} \cdot \Phi_{\text{flux}}(\lambda, \xi) \right\} \quad (4)$$

where V is the grid cell volume, $\int d\lambda$ is a surface integral over cell faces and $\hat{\mathbf{x}}$ is a unit-vector normal to the cell face at λ .

Eq. (4) is a function of two distinct time-scales: $\overline{\tau_{\text{react}}}(t)$ and the grid-scale time, τ_{R} , associated with Φ_{flux} . Inspection of Eq. (4) reveals that the RH “evolution rate” predicted by the subgrid assumption $\tau_{\text{react}}(\mathbf{x}, t) \rightarrow \overline{\tau_{\text{react}}}(t)$ is consistent with Wang et al.’s response time $(1/\overline{\tau_{\text{react}}} + 1/\tau_{\text{R}})^{-1}$. Of central importance, the evaporation rate predicted by Eq. (4) is given solely by $\overline{\tau_{\text{react}}}$; the subgrid mixing time associated with advective-diffusive mixing, i.e. \mathbf{u} and κ , does not appear in (4). Also, since (4) is independent of the variability in the subgrid RH field it follows that the assumption of sub-grid homogeneity is a special case of this more general result. It must be emphasized that the independence of evaporation (reaction) rate and κ implied by Eq. (4) is specific to advective-diffusive reaction that is linear combined with $\tau_{\text{react}}(\mathbf{x}, t) \rightarrow \overline{\tau_{\text{react}}}(t)$; reaction rates for explicitly non-linear reactions will always depend on κ , regardless of the subgrid modeling assumptions employed.

The above results lead us to the following conclusion:

The evaporation rate of unmixed clear and cloudy air predicted by current S -resolving microphysical schemes in a grid cell with internal unresolved divergenceless advective-diffusive mixing depends on τ_{react} and is independent of τ_{eddy} .

This statement contradicts the conclusion of Sec. 2a. Moreover, it reveals the following dilemma. Both the InC&E assumption—as its name implies—and the resolved- S model of evaporation in the limit $\tau_{\text{react}} \rightarrow 0$ are considered to converge to the “fast reaction” limit of divergenceless advective-diffusive evaporation. Yet these two models predict different evaporation rates in this limit. We are faced with a C&E time-scale dilemma: a choice between two common subgrid cloud modeling

strategies that are, in some sense, archetypal, inherently inconsistent, and thus, unsatisfactory.

2c. Damköhler number

Of central importance in this work is the Damköhler number (Damköhler 1940)

$$D_a = \frac{\text{mixing time-scale}}{\text{reaction time-scale}},$$

which provides insight into the fundamental nature of mixing and evaporation in clouds. In what follows we choose to define D_a in terms of the in-cloud number concentration

$$D_a = 4\pi D_v \overline{N}_c \frac{r^2}{r+a} \tau_{\text{eddy}}, \quad (5)$$

where \overline{N}_c is the cloud-averaged (as opposed to grid-averaged) number concentration. This definition of reaction time-scale differs from $\overline{\tau_{\text{react}}}$ which involves the grid-averaged concentration, \overline{N} , but is advantageous because \overline{N}_c is often measured experimentally and is more easily estimated. An estimation of the range of D_a as defined in Eq. (5) provides insight into relative differences in evaporation rate predicted by PDF and resolved- S models.

Two contour plots of D_a are shown in Fig. 1 where standard Kolmogorov scaling provides the estimate, $\tau_{\text{eddy}} = 0.1\varepsilon^{-1/3}L^{2/3}$ with L the grid cell length and ε the kinetic energy dissipation rate. The plots indicate that D_a spans four orders of magnitude in the range 10^{-2} to 10^2 for a broad range of $\{L, \overline{N}_c, r\}$ values and $\varepsilon = 0.01 \text{ m}^2 \text{ s}^{-3}$. In particular, an indirect aerosol effect is observed with D_a increasing linearly with N at fixed r ($N^{2/3}$ at fixed q_l) as indicated by Eq. (5). The contour $D_a = 1$ —where we expect the PDF and resolved models to predict similar evaporation rates for small ϕ_{sub} —tends to run through a relatively narrow range of droplet sizes between 2 and 10 μm . For small drops $r \ll 2 \mu\text{m}$ the InC&E assumption predicts greater evaporation rates than resolved- S schemes while for large drops $r \gg 10 \mu\text{m}$ the resolved model predicts faster evaporation than the InC&E approach. Taken as a whole, Fig. 1 reiterates the seriousness of the C&E time-scale dilemma: evaporation rates predicted by subgrid PDF schemes that use the InC&E assumption and LES/CRM models that resolve S and ignore subgrid correlations may vary more than two orders of magnitude for realistic atmospheric conditions.

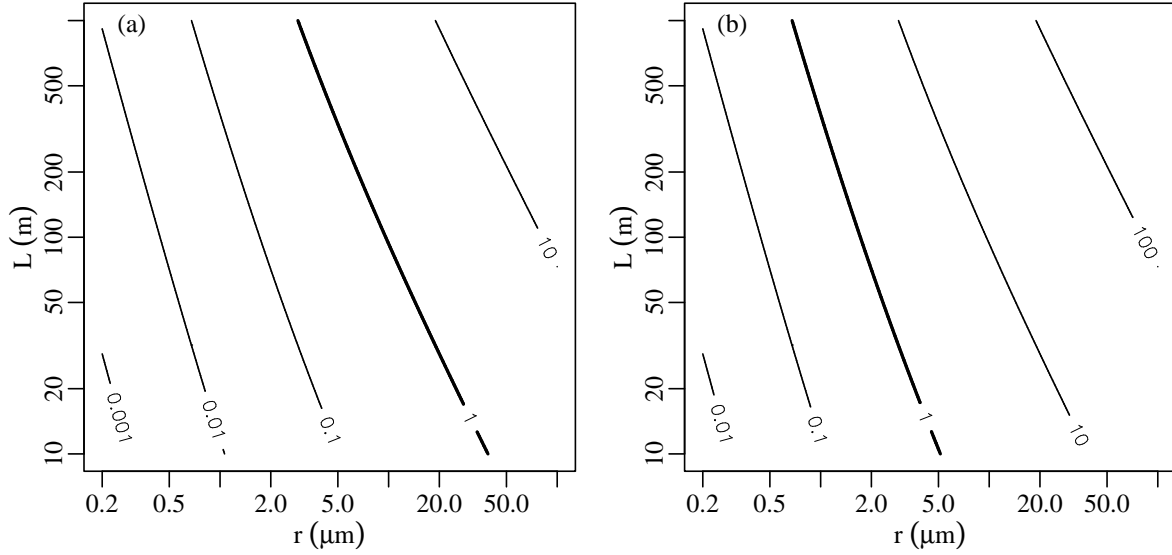


Figure 1: Contour plots of D_a as a function of $\{r, L\}$ for $N_c = 50 \text{ cm}^{-3}$ [Fig. 1(a)] and $N_c = 500 \text{ cm}^{-3}$ [1(b)], typical of clean marine and polluted marine/continental environments, respectively (Heymsfield and McFarquhar 2001). D_a is computed with Eq. (5), the Kolmogorov estimate $\tau_{\text{eddy}} = 0.1\epsilon^{-1/3}L^{2/3}$ and $\epsilon = 0.01 \text{ m}^2 \text{ s}^{-3}$. The figures reveal that a range of D_a values between 10^{-2} and 10^2 exist for typical atmospheric conditions and model grid sizes.

3. CLOUD FRONT EVAPORATION: EDDY-DIFFUSIVITY MODEL

In this section we investigate cloud front propagation and evaporation in a closed cell using a simple one-dimensional eddy-diffusivity model. A distinguishing feature of our cloud model is the assumption that droplet radius is time-independent. Although this assumption does not strictly conserve liquid water, it is appropriate for $\text{RH}_t > 1$, large drops and small subsaturations. The advantage of the constant radius assumption is that it leads to cloud front dynamics that are independent of the specifics of the droplet size distribution.

3a. Cloud model

The cloud model of interest is given by the following coupled PDEs:

$$\begin{aligned} \frac{\partial \text{RH}}{\partial t} &= \kappa_e \nabla^2 \text{RH} + \epsilon N (1 - \text{RH}) \\ \frac{\partial N}{\partial t} &= \kappa_e \nabla^2 N, \end{aligned} \quad (6)$$

with $\nabla \text{RH} = \nabla N = 0$ on the system boundaries, $\kappa_e \geq 0$ an eddy-diffusivity and $\epsilon \geq 0$ a constant. The C&E source term in the RH equation follows from

Eq. (3) using the time-independent droplet radius approximation $r(\mathbf{x}, t) = \text{constant}$. Following Grabowski (1993) and Majda and Souganidis (2000) we assume that the cloud ($\text{RH} = 1, N > 0$) and environmental air ($\text{RH} < 1, N = 0$) initially occupy disjoint regions of space. Of course, the constant droplet radius assumption implies the asymptotic $\text{RH}(\mathbf{x}, t) \rightarrow 1$ as $t \rightarrow \infty$.

We consider two different sets of initial conditions: 1.Front simulations in which the system is divided into two adjacent regions of clear and cloudy air and 2.Front simulations with two equal-sized regions of cloudy air surrounding a region of clear air. As the names imply, 1.Front simulations exhibit a single front of cloudy air propagating across the system while two such fronts exist for 2.Front initial conditions. The initial system fraction of clear (cloudy) air is denoted by ϕ_{sub} ($1 - \phi_{\text{sub}}$). Following the introduction and discussion of Damköhler number in Sec. 2b we find $D_a = \epsilon \overline{N}_c \tau_{\text{eddy}}$ for Eqs. (6) with $\overline{N}_c = \overline{N} (1 - \phi_{\text{sub}})^{-1}$ such that $\tau_{\text{react}} / \tau_{\text{eddy}} = (1 - \phi_{\text{sub}})^{-1} D_a^{-1}$.

3b. Model predictions using $\tau_{\text{eddy}} \sim L^2 / \kappa_e$

A comparison of the RH e -folding time, τ_{efold} , predicted by Eqs. (6) is shown in Fig. 2 for $\phi_{\text{sub}} \in [0.05, 0.95]$. In this comparison the mixing time-scale is taken as

$\tau_{\text{eddy}} \sim L^2/\kappa_e$ where L is the size of the system domain. This definition of τ_{eddy} is consistent with the subgrid large-eddy turn-over time.

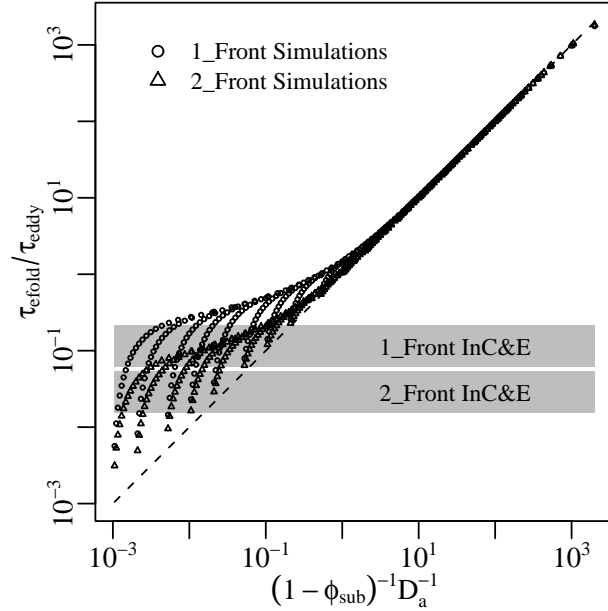


Figure 2: Plot of $\tau_{\text{efold}}/\tau_{\text{eddy}}$ as a function of $(1 - \phi_{\text{sub}})^{-1}D_a^{-1} = \tau_{\text{react}}/\tau_{\text{eddy}}$ predicted by Eqs. (6) with $\tau_{\text{eddy}} = 0.1L^2/\kappa_e$. Each “finger” in the lower left corner represent 21 different ϕ_{sub} values at fixed D_a with $\phi_{\text{sub}} \in [0.05, 0.95]$. The fingers are not visible in the upper right corner where rapid mixing implies $\tau_{\text{efold}} = \tau_{\text{react}}$ independent of ϕ_{sub} .

Figure 2 depicts two distinct regimes of evaporative behavior. For small $(1 - \phi_{\text{sub}})D_a$ [upper right corner], mixing occurs much faster than evaporation and $\tau_{\text{efold}} = \tau_{\text{react}}$ independent of τ_{eddy} . This is the high-resolution limit where the approximation $\tau_{\text{react}}(\mathbf{x}, t) = \overline{\tau_{\text{react}}}(t)$ is valid since the system is well-mixed for $t \gg \tau_{\text{eddy}}$. In contrast, for large $(1 - \phi_{\text{sub}})D_a$ [lower left corner] evaporation occurs faster than mixing and τ_{efold} appears to cluster in the range $\{0.01, 1\} \tau_{\text{eddy}}$ independent of τ_{react} . This is consistent with the behavior of subgrid PDF methods that use the InC&E assumption. We also find that τ_{efold} for the 2_Front simulations is persistently smaller at large D_a than the 1_Front τ_{efold} for a given $\{D_a, \phi_{\text{sub}}\}$. This behavior is expected since the 2_Front simulations have—as their name implies—approximately twice the interfacial area between clear and cloudy air for evaporation to occur.

To help clarify the relationship between predictions of the resolved- S and InC&E models and the behav-

ior of Eqs. (6), the predictions of these models are also shown in Fig. 2. The τ_{efold} predicted by resolved schemes is simply the 1-to-1 line (dashed) in the figure. It is more difficult to determine τ_{efold} predicted by the InC&E assumption since Eqs. (6) do not strictly conserve q_t . However, assuming that the constant radius approximation is consistent with a net change in q_t between 1 and 30% ($\Delta \ln r \in [0.003, 0.112]$) and integrating over ϕ_{sub} gives the two shaded regions in Fig. 2 as described in Appendix A. These additional comparisons reiterate that τ_{efold} predicted by Eqs. (6) is consistent with typical LES/CRM models for $(1 - \phi_{\text{sub}})D_a < 1$ and the InC&E assumption for $(1 - \phi_{\text{sub}})D_a > 1$, and inconsistent otherwise.

3c. Model predictions using $\tau_{\text{eddy}} \sim \text{var}(\text{RH})/\chi$

Inspection of Fig. 2 reveals an unsatisfactory aspect of the simulation results. Namely, τ_{efold} appears to exhibit a strong dependency on initial conditions, i.e. 1_Front vs 2_Front, for a given ϕ_{sub} . These subgrid initial conditions are, in general, unknown.

Motivated by the discussion of the InC&E assumption in Sec. 2a we introduce the mixing time-scale

$$\tau_{\text{eddy}} = \frac{1}{\tau_{\text{efold}}} \int_0^{\tau_{\text{efold}}} dt \frac{\text{var}(\text{RH})}{\chi}, \quad (7)$$

with scalar dissipation rate $\chi = \kappa_e |\nabla \text{RH}|^2$; Eq. (7) describes a time-averaged measure of the rate of RH variance erosion during advective-diffusive mixing. C&E time-scales for $\phi_{\text{sub}} \in [0.05, 0.95]$ are shown in Fig. 3 with τ_{eddy} given by Eq. (7).

Comparison of Figs. 2 and 3 reveals that $\text{var}(\text{RH})/\chi$ is a much more genuine measure of scalar mixing time than L^2/κ_e . Indeed, this should come as no surprise since χ is an essential quantity in the Oboukhov–Corrsin theory of turbulent advective-diffusive mixing (Tennekes and Lumley 1972, Chap. 8). However, it should be emphasized that Fig. 3 does *not* imply that τ_{efold} is independent of initial conditions. Rather, given a modeled or observed cloud-clear air interface that is complex and potentially self-similar (fractal), Fig. 3 reveals that just two well-defined statistical quantities— χ and $\text{var}(\text{RH})$ —form the foundation of the relationship between τ_{eddy} and the resolved (or observed) features of the interface.

3d. The Eddy Dissipation Concept (EDC) model

The results of Fig. 3 can be quantified, to first approximation, by the simple expression

$$\tau_{\text{efold}} = \max\{0.35\tau_{\text{eddy}}, \tau_{\text{react}}\}, \quad (8)$$

with τ_{eddy} given by Eq. (7). Equation (8) is also valid—but less accurate—for $\tau_{\text{eddy}} \sim L^2/\kappa_e$.

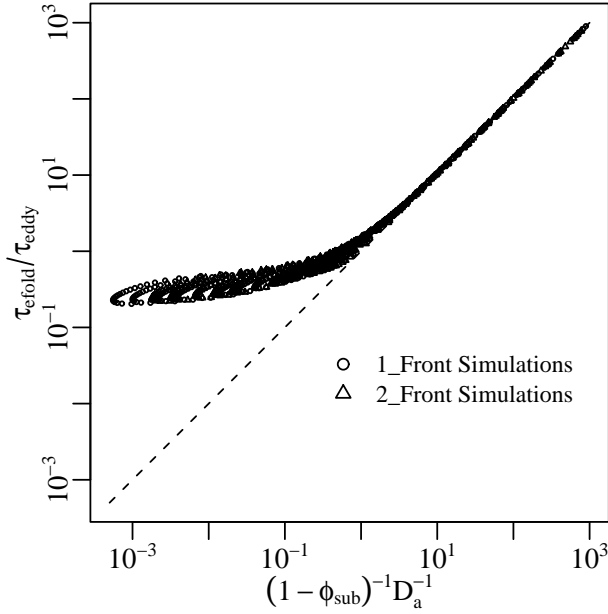


Figure 3: Plot of τ_{efold}/τ_{eddy} as a function of $(1 - \phi_{sub})^{-1}D_a^{-1}$ predicted by Eqs. (6) with τ_{eddy} given by Eq. (7). Comparison of Fig. 2 and 3 reveals that the diagnosis of τ_{eddy} from χ provides a superior estimate than $\tau_{eddy} \sim L^2/\kappa_e$.

Equation (8) resolves the C&E time-scale dilemma described in Sec. 2b. Neither τ_{eddy} predicted by resolved- S schemes nor the InC&E assumption are uniformly valid. Rather, the resolved model is valid for $(1 - \phi_{sub})D_a < 1$ and the InC&E assumption for $(1 - \phi_{sub})D_a > 1$.

Equation (8), albeit unexplored by the cloud physics community, is not new. In the combustion community, Eq. (8) is typically referred to as the Eddy Dissipation Concept (EDC) model. It is due to Magnussen and Hjertager (1976) who originally used $\tau_{eddy} \sim K/\varepsilon$ where K is kinetic energy. A variant of Eq. (8) was suggested earlier by Spalding (1971). The important role of χ in the evaluation of τ_{eddy} was first emphasized by Bilger (1976) in the fast chemistry limit, $D_a \rightarrow \infty$.

A quotation from Magnussen and Hjertager (1979), reproduced at the start of this manuscript, provides a physical interpretation of EDC for the turbulent evolution of a two-phase (liquid-vapor) mixture injected into a hot gas stream at large D_a . Magnussen and Hjertager recognize that when the liquid-vapor mixture comes into contact with the hot gas, the liquid will rapidly evaporate ($\tau_{react} \rightarrow 0$). They conclude that the net evaporation rate *for the system* (τ_{efold}) is therefore controlled

by the rate at which the liquid-vapor mixes into the hot stream (τ_{eddy}). This is the fundamental nature of reactive advective-diffusive mixing at large D_a for the class of non-linear reaction types that includes C&E.

3e. EDC, Broadwell–Breidenthal and reaction type

The phenomenological model of Broadwell and Breidenthal (1982) is based on the reaction type $A+B \xrightarrow{k} C$ with reaction rate k , where the scalar mixing statics, e.g. the surface area per unit volume of interface between the two reactants, are assumed k -independent. In contrast, mixing of cloudy and clear air with $\overline{RH}_t > 1$ is consistent with the reaction type $A+B \xrightarrow{k} B$ where A (B) represents subsaturated (saturated) air, respectively. In this case, the scalar mixing statics are strongly k -dependent at large D_a because a faster evaporation rate enhances the RH gradients across the cloud front which, in turn, affects the statistics of the (centimeter-scale) filaments where evaporation is occurring. This cloud-front sharpening is revealed in the cumulative probability density function (CDF) that $RH_{env} + \epsilon < RH < 1 - \epsilon$ with $0 < \epsilon \ll 1 - RH_{env}$ which is a measure of the volume fraction of RH-filaments when $\nabla\kappa_e = 0$.

A plot of the CDF averaged over τ_{efold} is shown in Fig. 4 for the simulations of Sec. 3c and $\epsilon = 0.01(1 - RH_{env})$. As in Fig. 3, two distinct regimes are evident in the small and large D_a limits. For small $(1 - \phi_{sub})D_a$, the average system state is well-mixed and hence the “filament” where evaporation is occurring is the entire system volume. In contrast, at large $(1 - \phi_{sub})D_a$ the front sharpening process decreases the volume fraction of filaments with increasing D_a . This behavior—valid for $\overline{RH}_t > 1$ —contradicts the Broadwell–Breidenthal model where the filament statistics are assumed to be independent of τ_{react} , and hence D_a .

3f. EDC and Reynolds decompositions

To conclude this section, it is of interest to recast the subgrid approximation $\tau_{react}(\mathbf{x}, t) = \overline{\tau_{react}}(t)$ of Sec. 2b in terms of a Reynolds decomposition of subgrid quantities (Cooper 1989; Stevens et al. 1998). Denoting centered fluctuating variables with a prime, this approximation is rewritten $\overline{S'\tau_{react}'} = 0$, in general, or $\overline{N'S'} = 0$ for the constant radius approximation considered here.

There are two normalizing coefficients of interest, $c \in \{c_1, c_2\}$, such that $c\overline{N'S'}$ is non-dimensional. The first, $c_1 = (\sigma_N\sigma_S)^{-1}$ gives the standard correlation coefficient $\rho_1 \in [-1, 1]$ where σ_X is the standard deviation of quantity X . Not surprisingly, N and S are highly correlated with $\rho_1 \approx 1$ independent of D_a (not shown). The second coefficient, $c_2 = (\overline{N|S'})^{-1}$ pro-

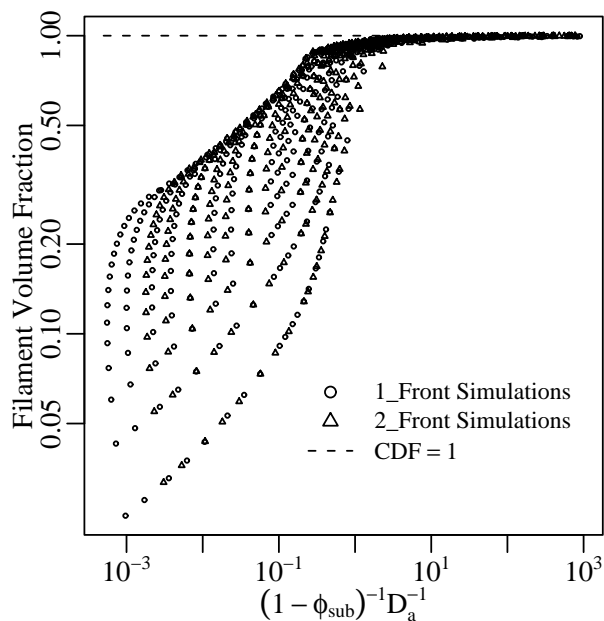


Figure 4: Plot of the cumulative probability that $\text{RH}_{\text{env}} + \epsilon < \text{RH} < 1 - \epsilon$, averaged over τ_{efold} and predicted by the 1_Front and 2_Front simulations of Sec. 3c with $\epsilon = 0.01(1 - \text{RH}_{\text{env}})$. The figure shows increasing RH-front sharpening with increasing D_a .

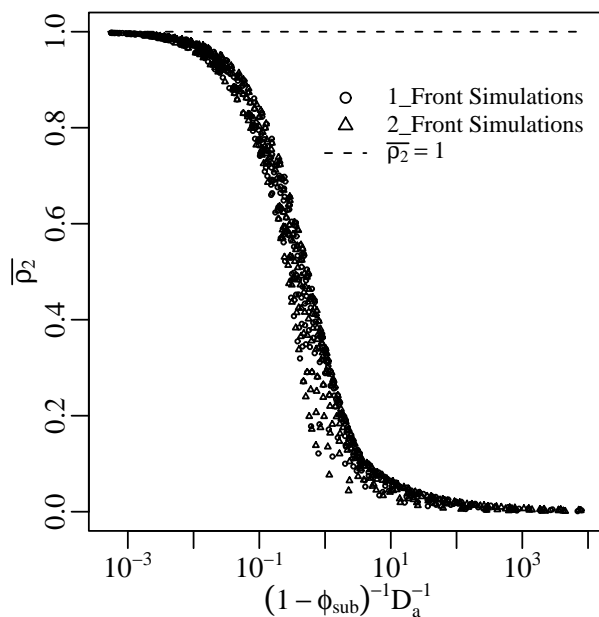


Figure 5: Plot of the correlation coefficient, $\rho_2 = \overline{N'S'}/(\overline{N|S|})$, averaged over τ_{efold} and predicted by the 1_Front and 2_Front simulations of Sec. 3c. The correlation $\overline{N'S'}$ appears in the evolution equation for $\overline{\text{RH}}$ and acts to increase τ_{efold} at large D_a .

vides a correlation coefficient ρ_2 that is a measure of the relative importance of the covariance $\overline{N'S'}$. In particular, $\rho_2(t = 0) = 1$ for the “cloud-front” initial conditions used in this section and $\rho_2(t \rightarrow \infty) = 0$ for the well-mixed final state.

A plot of ρ_2 averaged over τ_{efold} is shown in Fig. 5 for the simulations of Sec. 3c. The results of this figure are consistent with and compliment the results of Fig. 3. For $(1 - \phi_{\text{sub}})D_a > 1$, $\overline{N'S'}$ is of relative importance (Fig. 5) and neglect of this covariance leads to a dramatic underestimation of τ_{efold} (Fig. 3). This behavior reiterates that LES/CRM models which resolve S and assume $\overline{N'S'} = 0$ overestimate evaporation at large D_a .

4. A TEST OF EDC: SPURIOUS CLOUD-EDGE SUPERSATURATIONS

We showed in Sec. 3 that LES/CRM models using the approximation $\tau_{\text{react}}(\mathbf{x}, t) = \overline{\tau_{\text{react}}}(t)$ underestimate τ_{efold} and therefore overestimate cloud front evaporation at large Damköhler numbers. Enhanced numerical prediction of C&E at cloud edges—and resulting

instabilities—was first studied by Klaassen and Clark (1985). Subsequent work focused on the application of monotonic advection schemes to mitigate these instabilities (Grabowski 1989; Grabowski and Smolarkiewicz 1990; Grabowski and Clark 1991). But not until the study of Stevens et al. (1996), was a purely non-advective mechanism for spurious cloud-edge supersaturation exposed.

Stevens et al. consider the non-diffusive propagation of a cloud front across a 1D grid cell at constant velocity (U) as described by the triplet $\{\theta_l, q_t, r\}$. Following past studies they investigate the evolution of the corresponding grid-cell averaged quantities $\{\Theta_l, Q_t, R\}$ with one novel difference—Stevens et al. diagnose the grid-scale advective tendency without approximation, i.e. $U\nabla\psi = \overline{U\nabla\psi}$ where the pair $\{\Psi, \psi\}$ is one of the three thermodynamic parameters. By assuming that advection can be performed perfectly at the grid-scale, the effect of subgrid modeling assumptions is, thereby, isolated. The Stevens et al. scenario, generalized to include turbulent eddy-diffusive mixing, provides an additional framework to study the effectiveness of the EDC model.

4a. Modified Stevens et al. model

Stevens et al. observe large fluctuations in $\overline{\text{RH}}$ when C&E at the grid-scale is evaluated using $\{\Theta_l, Q_l, R\}$. As shown in their Fig. 3(b), supersaturations reach 4% and, quite counter-intuitively, supersaturation oscillations increase with *decreasing* τ where τ is the time required for the cloud front to propagate across the grid cell. Stevens et al. attribute these large fluctuations in S to the logical consequence of driving microphysical forcings with grid-averaged supersaturations. However, there is an additional forcing in their study that is causing S to exceed 1%, namely, the approximation $Q_l \sim R^3$ [their Eq. (4)] used in the calculation of T from $\Theta_l(Q_l)$. The exact advective tendencies of $\{Q_l, R\}$ are linear in time while the approximation $Q_l \sim R^3$ gives $Q_l \sim t^3$, an underestimation as seen in their Fig. 3(d). By underestimating the advective tendency of Q_l , Stevens et al. underestimate T [Fig. 3(a)] and overestimate RH [Fig. 3(b)], independent of C&E.

We consider evolution of the triplet $\{\Theta_l, Q_l, R\}$ with advective tendencies evaluated exactly from $\{\theta, q_t, q_l\}$ such that the diagnosed advective tendency of T is linear in time.[†] In addition, we extend Stevens et al.'s laminar problem by adding eddy-diffusive mixing:

$$\frac{\partial \Psi}{\partial t} = -\overline{U \nabla \psi} + \kappa_e \overline{\nabla^2 \psi},$$

for $\Psi \in \{\Theta_l, Q_l\}$ where

$$\psi(x, t) = \Psi_e + \frac{(\Psi_c - \Psi_e)}{2} \operatorname{erfc} \left(\frac{x - Ut}{\sqrt{4\kappa_e t}} \right)$$

is the analytic solution for the evolution of a cloud-edge initialized at $(x = 0, t = 0)$, and Ψ_c (Ψ_e) represents unmixed cloud (clear) values.

In contrast, Q_l is evaluated numerically according to

$$\frac{\partial Q_l^{(n)}}{\partial t} = -\overline{U \nabla q_l} + \kappa_e \overline{\nabla^2 q_l} + \overline{\mathcal{F}^{(n)}}, \quad (9)$$

where $\overline{\mathcal{F}^{(n)}}$, $n \in \{1, 2, 3\}$ represents three different grid-scale microphysical forcings:

$$\begin{aligned} \overline{\mathcal{F}^{(1)}} &= \frac{dQ_l}{dt} \left\{ R \sim Q_l^{1/3} \right\} \\ \overline{\mathcal{F}^{(2)}} &= \mathcal{L} \frac{dQ_l}{dt} \left\{ R \sim Q_l^{1/3} \right\} \\ \overline{\mathcal{F}^{(3)}} &= \mathcal{L} \frac{dQ_l}{dt} \left\{ R \sim Q_l^{1/3} (1 - \phi_{\text{sub}})^{2/3} \right\}, \end{aligned}$$

and $\mathcal{L} = \tau_{\text{react}} / \max(\tau_{\text{eddy}}, \tau_{\text{react}})$ when $dQ_l/dt < 0$ and 1 otherwise. Specifically, $\overline{\mathcal{F}^{(1)}}$ denotes the usual

grid-scale averaged C&E-forcing with diagnostic relation $R \sim Q_l^{1/3}$ *overestimating* droplet radius, $\overline{\mathcal{F}^{(2)}}$ denotes the evaporation-limiting EDC model also with $R \sim Q_l^{1/3}$, and $\overline{\mathcal{F}^{(3)}}$ denotes the EDC model with improved diagnosis of R . Straightforward substitution verifies that the evaporation limiter, \mathcal{L} , produces EDC behaviour in the RH-equation that agrees with Eq. (8). We diagnose grid-cell cloud fraction crudely according to $\phi_{\text{sub}}(t) = (\Psi_c - \Psi) / (\Psi_c - \Psi_e)$; this definition of ϕ_{sub} is exact for $\kappa_e = 0$, questionable otherwise. Explicit relations for dQ_l/dt and τ_{react} are given in Appendix B.

In our implementation of the EDC model described above and in Appendix B, no attempt is made to “tune” the evaporation limitation via a constant of proportionality that relates τ_{efold} and τ_{eddy} , e.g. as per Eq. (8). Rather, our aim is to provide a first-order assessment of the efficacy of the EDC model in a mixing scenario that includes advection and cross-grid transport, and that is distinct from Sec. 3. Consistent with the treatment of advection-diffusion (above), the EDC model is applied at each time step with $\tau_{\text{eddy}}(t) = \text{var}(\text{RH})/\chi$ calculated “exactly” from the fully-resolved subgrid field.

In Stevens et al. (1996)'s original scenario the single time-scale $\tau = L/U$ describes the purely advective transport across the grid cell; the addition of diffusion, here, introduces a second time-scale $\tau_\kappa = L^2/\kappa_e$. Since, our analysis continues to use τ as the primary time-scale we consider only $N_\kappa \leq 0.1$ where $N_\kappa \equiv \tau/\tau_\kappa$ is a non-dimensional measure of the relative importance of diffusion.

4b. Results

Plots comparing $\{\overline{\text{RH}}, \overline{\text{RH}}^{(1)}, \overline{\text{RH}}^{(3)}\}$ and $\{\overline{q_l}, Q_l^{(1)}, Q_l^{(3)}\}$ as functions of t/τ for each $N_\kappa \in \{0, 0.01, 0.1\}$ are shown in Fig. 6. Before considering the impact of EDC on grid-averaged quantities, it is of interest to assess differences in $\overline{\text{RH}}^{(1)}$ for $\kappa_e = 0$ between the present approach and Stevens et al., as seen in their Fig. 3(b). The grid-averaged supersaturation, $\overline{\text{RH}}^{(1)} - 1$, gently plateaus near 0.2% in the current approach, while Fig. 3(b) in Stevens et al. shows a pronounced supersaturation peak that reaches 1.5%. As discussed in the previous subsection, the cause of the enhanced supersaturation oscillation in their work is the approximation $Q_l \sim R^3$ which causes grid-average temperatures to be underestimated. Consequently, $\overline{\text{RH}}^{(1)}$ converges to $\overline{\text{RH}}$ in the limit $\tau \rightarrow 0$ in the present approach but the opposite behavior is exhibited in Stevens et al.'s Fig. 3(b).

Fig. 6 also demonstrates the effect of the EDC model on grid-cell averaged quantities with R diagnosed from

[†]Note that $\exp\{-L_v Q_l / (c_p a T)\} = 1 - L_v Q_l / (c_p a T)$ to good approximation for the thermodynamic parameters used in Stevens et al. and here.

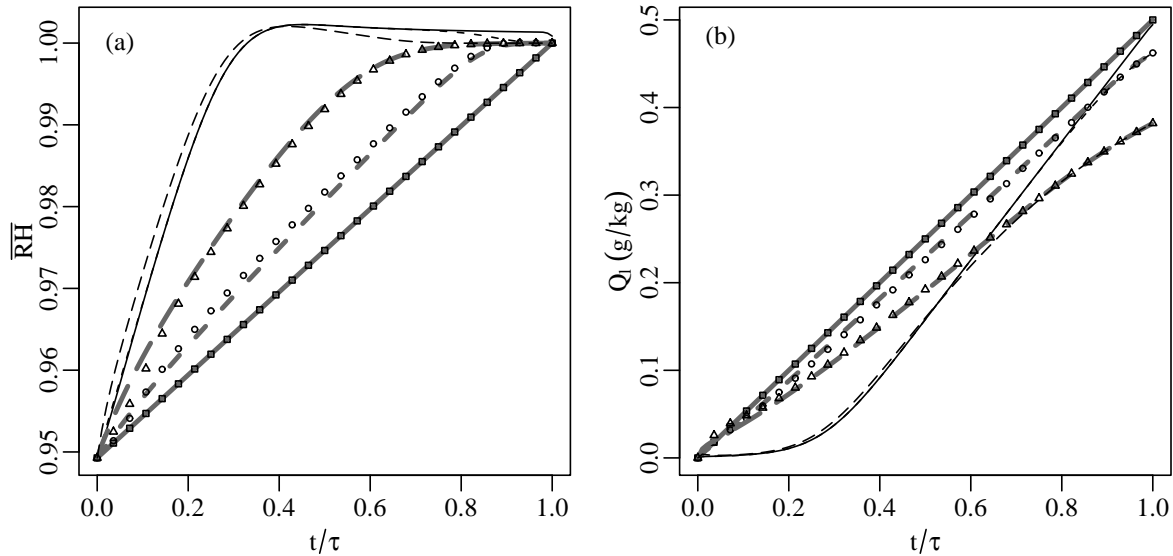


Figure 6: Comparison of $\overline{\text{RH}}$ [Fig. 6(a)] and Q_l [Fig. 6(b)] diagnosed exactly from the resolved subgrid field (thick lines) and computed using grid-cell averaged microphysical forcing with evaporation limitation ($\overline{\mathcal{F}}^{(3)}$ in Eq. (9); symbols) and without ($\overline{\mathcal{F}}^{(1)}$ in Eq. (9); thin lines). Line and symbol types represent different N_{κ} values: $\{\text{—}, \square\}$ is $N_{\kappa} = 0$, $\{-\text{-}, \circ\}$ is $N_{\kappa} = 0.01$, and $\{-\cdot\cdot, \triangle\}$ is $N_{\kappa} = 0.1$. Evaporation limitation based on the EDC model produces $\{\overline{\text{RH}}, Q_l\}$ evolution that agrees closely with the resolved subgrid field. Calculations performed with $\tau = 181$ s and parameter value from Stevens et al. (1996, Table 1). Note that the thin solid line overlays the thin dashed line for $t < 0.8\tau$.

$Q_l^{1/3}(1 - \phi_{\text{sub}})^{2/3}$. Qualitatively, the agreement between $\{\overline{\text{RH}}^{(3)}, Q_l^{(3)}\}$ and $\{\overline{\text{RH}}, \overline{q_l}\}$ is very good. In particular, EDC limits the large evaporation rates that otherwise cause oscillations in the supersaturation field. In fact, for the original Stevens et al. scenario with $\kappa_e = 0$, the predictions of the EDC model are exactly correct. Essentially, this is a trivial limit of the EDC model in 1D where $\tau_{\text{efold}} \rightarrow \infty$ as $\kappa_e \rightarrow 0$. A quantitative assessment of the accuracy of EDC is found in Jeffery and Reisner (2006).

4c. Summary

Stevens et al. construct a novel scenario of purely advective cloud front propagation across a grid cell in 1D where spurious oscillations are observed in the grid-scale prognostic variables $\{\Theta_l, Q_t, R\}$. They do not suggest a solution to this problem.

We have shown that the EDC model exactly solves the non-turbulent problem articulated by Stevens et al.—and appears to provide good results for the more general turbulent case—with three important caveats:

- Stevens et al. use the approximation $Q_l \sim R^3$ in

the determination of temperature which introduces a second grid-scale forcing that is independent of C&E. We avoid this forcing by using a different prognostic triplet, $\{\Theta_l, Q_t, Q_l\}$.

- The accuracy of EDC for $\kappa_e > 0$ depends, in turn, on the accuracy of the subgrid parametrization for τ_{eddy} . Good results using $\tau_{\text{eddy}} = 0.05L^2/\kappa_e$ for the present scenario suggest that reasonably accurate diagnosis of τ_{eddy} , while difficult, is feasible.
- The surrogate problem for 3D turbulent transport tested here—advection and eddy-diffusion in 1D—is of limited complexity. In particular, incompressible advection is confined to a constant and trivial mean sweep in 1D. EDC has yet to be tested in 3D where advection plays a dominant role in cascading variance from large to small scales.

5. SUMMARY

Prediction of the turbulent evolution of a mixture of clear and cloudy air is, fundamentally, a Lagrangian problem that is of higher dimension than that of typical reactive

scalar systems. The interaction of a droplet with the surrounding temperature and vapor fields depends, in particular, on the droplet radius which is expressed as a Lagrangian path integral along droplet trajectories. This reveals an essential difficulty in predicting droplet spectral evolution—and hence evaporation—at unresolved scales.

In this work we exploit a time-independent droplet radius approximation—appropriate for $\text{RH}_t > 1$, large drops and small subsaturations—that essentially removes the Lagrangian character from the problem at hand. In particular, this assumption implies that cloud front propagation and evaporation is independent of the specifics of the droplet size distribution and a function of only two time-scales, τ_{react} and τ_{eddy} . Two common cloud schemes (i) PDF schemes that exploit the InC&E assumption and (ii) LES/CRM schemes that resolve τ_{react} and ignore subgrid correlations make diametric assumptions $\tau_{\text{efold}} \sim \tau_{\text{eddy}}$ and $\tau_{\text{efold}} \sim \tau_{\text{react}}$, respectively. We are faced with a C&E time-scale dilemma: a choice between two common subgrid cloud modeling strategies that are, in some sense, archetypal, inherently inconsistent, and thus, unsatisfactory.

The resolution to the C&E time-scale dilemma is found in the pioneering work of Magnussen and Hjertager (1976) who first hypothesized the relation $\tau_{\text{efold}} \sim \max(\tau_{\text{eddy}}, \tau_{\text{react}})$ which encapsulates the behavior of traditional PDF and resolved C&E schemes at different limits. We have verified using two very different conceptual approaches—1D eddy-diffusivity modeling and a new PDF approach with resolved C&E—that Magnussen and Hjertager’s EDC model correctly predicts the evaporation rate for cloud-front propagation across a grid-cell in the constant radius limit and in the absence of sedimentation and inertial effects. These results imply that PDF schemes overestimate evaporation at small Damköhler number while LES/CRM models that resolve C&E overestimate evaporation at large D_a .

Although the estimate $D_a \sim L^{2/3}$ might suggest that PDF and LES/CRM schemes are correct in typical small and large grid size limits, respectively, Fig. 1 demonstrates otherwise. For example, at 20 m resolution, the resolved- S approximation used by many LES/CRM models $\tau_{\text{efold}} \sim \tau_{\text{react}}$ becomes invalid at r greater than about $50 \mu\text{m}$ and $\overline{N}_c = 50 \text{ cm}^{-3}$; at $\overline{N}_c = 500 \text{ cm}^{-3}$ the resolved- S approximation breaks down near $5 \mu\text{m}$. In a similar fashion, PDF schemes that utilize the InC&E assumption are not uniformly valid at $L = 1000 \text{ m}$ and typical atmospheric conditions. These results reiterate and substantiate concerns that have been raised in the cloud physics literature that modeled evaporation rates are too high (Krueger 1993; Stevens et al. 1996), or more gener-

ally, are of particular importance to overall model performance (Stevens et al. 2005).

Implementation of the EDC model in high-resolution schemes requires modifying the C&E source term for dq_l/dt with the evaporation limiter $\mathcal{L} = \tau_{\text{react}} / \max(c_1 \tau_{\text{eddy}}, \tau_{\text{react}})$ when $dq_l/dt < 0$; direct substitution verifies that \mathcal{L} correctly reproduces the EDC behavior $\tau_{\text{efold}} \sim \max(\tau_{\text{eddy}}, \tau_{\text{react}})$ in the RH-equation and constant radius limit. Our numerical simulations suggest $c_1 \approx 0.35$. This new scheme additionally requires the diagnosis of (subgrid) τ_{eddy} from the resolved field. We have tested this implementation of EDC with diagnostic relation $\tau_{\text{eddy}} = c_2 L^2 / \kappa_e$ in a turbulent generalization of the Stevens et al. (1996) scenario of 1D cloud front propagation and find very good quantitative results for $c_2 = \mathcal{O}(0.1)$. This result is encouraging because L and κ_e are already standard computed quantities in many LES/CRM models.

Acknowledgement This work was funded by a Los Alamos National Laboratory Directed Research and Development Project entitled “Resolving the Aerosol-Climate-Water Puzzle (20050014DR)”.

A. THE InC&E ASSUMPTION AND CLOUD EVAPORATION

The analog of Eqs. (6) for subgrid PDF schemes that use the InC&E assumption is

$$\begin{aligned} \frac{\partial \text{RH}_t}{\partial t} &= \kappa_e \nabla^2 \text{RH}_t \\ \text{RH} &= \min(1, \text{RH}_t), \end{aligned} \quad (10)$$

with $\overline{q_l} \sim \overline{\Gamma(\text{RH}_t - 1)(\text{RH}_t - 1)}$ where Γ is a step function. To generate the shaded regions in Fig. 2, Eqs. (10) are first solved using 1.Front and 2.Front initial conditions for $\Delta \overline{q_l} \in [0.01, 0.30] \overline{q_l}$ and a distribution of ϕ_{sub} . The range of τ_{efold} shown in Fig. 2 is then calculated by averaging over ϕ_{sub} .

B. MICROPHYSICAL RELATIONS FOR SEC. 4

Let

$$\frac{dQ_l}{dt} = 4\pi \frac{\rho_w}{\rho_a} \overline{N}_c \mathcal{R}^2 \frac{d\mathcal{R}}{dt},$$

with

$$\begin{aligned} \frac{d\mathcal{R}}{dt} &= c_r Q_s \frac{\rho_a}{\rho_w} D_v \frac{\overline{\text{RH}} - 1}{\mathcal{R} + a} \\ c_r &= \left\{ 1 + \frac{D_v}{D_a} \left(\frac{L_v}{R_v T} - 1 \right) \frac{L_v}{c_{p,a} T} Q_s \right\}^{-1}, \end{aligned}$$

and parameter values $\overline{N_c} = 100 \text{ cm}^{-3}$, $a = 2 \text{ }\mu\text{m}$, and thermodynamics parameters as in standard texts (Pruppacher and Klett 1997).

Then the diagnosis of \mathcal{R} in $\overline{\mathcal{F}}^{(1-3)}$ obeys

$$\begin{aligned}\overline{\mathcal{F}}^{(1-2)} &\rightarrow \mathcal{R} = R \\ \overline{\mathcal{F}}^{(3)} &\rightarrow \mathcal{R} = R(1 - \phi_{\text{sub}})^{2/3},\end{aligned}$$

with

$$R = \left(\frac{3}{4\pi} \frac{\rho_a}{\rho_w} \frac{Q_l}{\overline{N_c}} \right)^{1/3},$$

and

$$\tau_{\text{react}} = \frac{1}{4\pi D_v \overline{N_c}} \frac{\mathcal{R} + a}{\mathcal{R}^2}.$$

REFERENCES

- Bilger, R. W., 1976: The structure of diffusion flames. *Combust. Sci. and Tech.*, **13**, 155–170.
- Broadwell, J. E. and R. E. Breidenthal, 1982: A simple model of mixing and chemical reaction in a turbulent shear layer. *J. Fluid Mech.*, **125**, 397–410.
- Cooper, W. A., 1989: Effects of variable droplet growth histories on droplet size distributions. Part I: Theory. *J. Atmos. Sci.*, **46**, 1301–1311.
- Damköhler, G. Z., 1940: Influence of turbulence on flame velocity in gaseous mixtures. *ZH Electrochem*, **46**, 601.
- Grabowski, W. W., 1989: Numerical experiments on the dynamics of the cloud-environment interface: Small cumulus in a shear-free environment. *J. Atmos. Sci.*, **46**, 3513–3541.
- 1993: Cumulus entrainment, fine-scale mixing, and buoyancy reversal. *Quart. J. Roy. Meteor. Soc.*, **119**, 935–956.
- Grabowski, W. W. and T. L. Clark, 1991: Cloud-environment interface stability: Rising thermal calculations in two spatial dimensions. *J. Atmos. Sci.*, **48**, 527–546.
- Grabowski, W. W. and P. K. Smolarkiewicz, 1990: Monotone finite-difference approximations to the advection-condensation problem. *Mon. Wea. Rev.*, **118**, 2082–2097.
- Heymsfield, A. J. and G. M. McFarquhar, 2001: Microphysics of INDOEX clean and polluted trade cumulus clouds. *J. Geophys. Res.*, **106**, 28653–28673.
- Jeffery, C. A. and P. H. Austin, 2003: Unified treatment of thermodynamic and optical variability in a simple model of unresolved low clouds. *J. Atmos. Sci.*, **60**, 1621–1631.
- Jeffery, C. A. and J. M. Reisner, 2006: A study of cloud mixing and evolution using PDF methods. 1. Cloud front propagation and evaporation. *J. Atmos. Sci.*, in press.
- Klaassen, G. P. and T. L. Clark, 1985: Dynamics of the cloud-environment interface and entrainment in small cumuli: Two-dimensional simulations in the absence of ambient shear. *J. Atmos. Sci.*, **42**, 2621–2642.
- Krueger, S. K., 1993: Linear eddy modeling of entrainment and mixing in Stratus clouds. *J. Atmos. Sci.*, **50**, 3078–3090.
- Lohmann, U. and J. Feichter, 2005: Global indirect aerosol effects: a review. *Atmos. Chem. Phys.*, **5**, 715–737.
- Magnussen, B. F. and B. H. Hjertager, 1976: On mathematical modeling of turbulent combustion with special emphasis on soot formation and combustion. *Sixteenth Symposium (International) on Combustion*, Pittsburgh, Pa : Combustion Institute, Cambridge, MA, USA, 719–729.
- 1979: Calculation of flow, mixing, and evaporation of a two-phase mixture injected into a hot gas stream. *Two-phase Momentum, Heat and Mass Transfer in Chem, Process, and Energy Eng Syst*, Washington, DC : Hemisphere Publ Co, Dubrovnik, Yugosl, 411–422.
- Majda, A. and P. Souganidis, 2000: The effect of turbulence on mixing in prototype reaction-diffusion systems. *Comm. Pure Appl. Math.*, **53**, 1284–1304.
- Mellor, G. L., 1977: The Gaussian cloud model relations. *J. Atmos. Sci.*, **34**, 356–358, see also CORRIGENDA, **34**, 1483.
- Pruppacher, H. R. and J. D. Klett, 1997: *Microphysics of Clouds and Precipitation*. Kluwer Academic, Boston, MA, USA, 2nd edition.
- Sommeria, G. and J. W. Deardorff, 1977: Subgrid-scale condensation in models of nonprecipitating clouds. *J. Atmos. Sci.*, **34**, 344–355.
- Spalding, D. B., 1971: Mixing and chemical reaction in steady confined turbulent flames. *Thirteenth Symposium (International) on Combustion*, Pittsburgh, Pa : Combustion Institute, 649–657.

- Squires, P., 1952: The growth of cloud drops by condensation. 1. General characteristics. *Aust. J. Sci. Res.*, **A5**, 59–86.
- Stephens, G. L., 2005: Cloud feedbacks in the climate system: A critical review. *J. Climate*, **18**, 237–273.
- Stevens, B., W. R. Cotton, and G. Feingold, 1998: A critique of one- and two-dimensional models of boundary layer clouds with a binned representations of drop microphysics. *Atmos. Res.*, **47-48**, 529–553.
- Stevens, B., C.-H. Moeng, A. S. Ackerman, C. S. Bretherton, A. Chlond, S. De Rhoode, and J. Edwards, 2005: Evaluation of large-eddy simulations via observations of nocturnal marine stratocumulus. *Mon. Wea. Rev.*, **133**, 1443–1462.
- Stevens, B., R. L. Walko, and W. R. Cotton, 1996: The spurious production of cloud-edge supersaturations by Eulerian models. *Mon. Wea. Rev.*, **124**, 1034–1041.
- Tennekes, H. and J. L. Lumley, 1972: *A First Course in Turbulence*. MIT Press, Cambridge, Massachusetts and London, England.
- Wang, S., Q. Wang, and G. Feingold, 2003: Turbulence, condensation, and liquid water transport in numerically simulated nonprecipitating Stratocumulus clouds. *J. Atmos. Sci.*, **60**, 262–278.